Studies of Black Silicon and Black Diamond as materials for antibacterial surfaces

G. Hazell[1], P. W. May[2,†], P. Taylor[2], A. H. Nobbs[1], C. C. Welch[3], B. Su[1].

[1] Bristol Dental School, University of Bristol, Lower Maudlin Street, Bristol, BS1 2LY, United Kingdom

[2] School of Chemistry, University of Bristol, Bristol BS8 1TS, United Kingdom.

[3] Oxford Instruments Plasma Technology, Yatton, Bristol BS49 4AP, United Kingdom.

[†] Corresponding author.

Keywords: black silicon, black diamond, antibacterial surfaces

1. Abstract

'Black silicon' (bSi) samples with surfaces covered in nanoneedles of varying length, areal density and sharpness, have been fabricated using a plasma etching process. These nanostructures were then coated with a conformal uniform layer of diamond using hot filament chemical vapour deposition to produce 'black diamond' (bD) surfaces. The effectiveness of these bSi and bD surfaces in killing Gram-negative (*E. coli*) and Gram-positive bacteria (*S. gordonii*) was investigated by culturing the bacteria on the surfaces for a set time and then measuring the live-to-dead ratio. All the nanostructured surfaces killed *E. coli* at a significantly higher rate than the respective flat Si or diamond control samples. The length of the needles was found to be less important than their separation, *i.e.* areal density. This is consistent with a model for mechanical bacteria death based on the stretching and disruption of the cell membrane, enhanced by the cells motility on the surfaces. In contrast, *S. gordonii* were unaffected by the nanostructured surfaces, possibly due to their smaller size, thicker cell membrane and/or their lack of motility.

2. Introduction

Diamond films grown by chemical vapour deposition (CVD) [1] are finding an increasing number of applications due to the extreme properties of diamond together with their rising availability and affordability from a number of commercial suppliers. Doping the diamond with boron allows the film conductivity to be varied controllably from insulating to near-metallic [2]. As a result, boron-doped diamond (BDD) has begun to find applications as electrochemical electrodes for electroanalysis [3,4], water treatment [5], neural interfacing [6], substrates for cell growth [7] and in supercapacitor fabrication [8]. Structuring the diamond surface on the micro- or nanoscale can greatly increase the effective electrode surface area, leading to higher sensitivity, increased selectivity, and higher capacitance values [9,10]. We recently reported [11] a method to fabricate high-surface-area BDD electrodes using so-called 'black silicon' (bSi) as a template. Black Si is a synthetic nanostructured material that contains high-aspect-ratio nanoprotrusions, such as nanospikes or nanoneedles, on its surface produced through plasma etching. The formation mechanism is not fully understood, but it is believed that particulates from the chamber sidewall, or ones that have homogeneously nucleated in the gas phase, deposit onto the Si wafer surface and act as micromasks. A highly anisotropic etch process then etches the Si into high-aspect-ratio needles. The name 'black silicon' originates from its deep black colour, resulting from the absorption of >99% of the visible light falling onto its surface. Originally something to be avoided, bSi has now found applications in photovoltaics [12,13] and has recently been used for biomedical sensing applications [14,15].

As well as having excellent electrochemical properties, we recently reported [11] that the spikey BDD-coated bSi surface, which we call 'black diamond' (bD), generated a mechanical bactericidal effect, killing the Gram-negative bacterium *Pseudomonas aeruginosa* at high rates. Uncoated bSi has also been reported to act as a bactericidal surface for both Gram-negative and Gram-positive bacteria [16], but the nanostructured bSi surface is rather delicate and easily damaged or scratched – even a human fingernail dragged across the surface would break and dislodge the needles. The advantage of the diamond coating is that the structures become far more robust and less likely to become damaged. In this case, the fingernail test did not cause any obvious damage to the bD needles. Previously we only investigated the efficacy of one type of bD, having a needle length of about 0.5 μm. Although some studies have been reported [17] on the bactericidal efficacy of other carbon nanostructured surfaces, such as carbon nanotubes and graphene, there are no reported studies in which the antimicrobial

properties of bD surfaces has been investigated systematically in terms of needle length, tip diameter and needle density.

There are currently three prevailing explanations for the bactericidal mechanism of nanostructured surfaces: (a) direct penetration of the cell membrane by nanofeatures [18], (b) bacterial cell adhesion and subsequent stretching and rupture of the membrane in between nanoprotrusions [19,20,21] or (c) membrane deformation due to cell adhesion to nanofeatures on a surface [22]. Xue *et al.* [20] and Li *et al.* [21] have considered such bactericidal mechanisms within the remit of 'stretching theory'. It is proposed that adhesion of a bacterial cell is dictated by both adhesion energy and the deformation energy of the cell membrane. In the mathematical model by Xue *et al.,* the effects of both gravity and van der Waals forces on cell-wall rupture were considered, with the conclusion that Gram-negative bacteria could be killed efficiently on nanopillared surfaces.

Experimental studies on various nanostructured surfaces have indicated that the length of the structures (*i.e.* needle or pillar length) is a factor in cell death [23]; however it is less important than might be expected. Wu *et al.* [24] have experimentally analysed the interactions of bacteria with nanostructured gold surfaces. They proposed that as the height of nanofeatures on the surface decreased, the features became more like "dots", resulting in reduced deformation/stretching of the bacterial cell membrane and thus lower percentage cell death. Thus, depending on the material and the size of the bacterium involved, there is a lower limit to the feature length for effective cell death. Death rate increases as feature length increases but only up to a certain point (usually a few μm), after which further increases in length provide no additional benefit as the cell membrane is already stretched to its maximum capacity.

The areal *density* (or pitch) of the nanofeatures is, however, a far more important parameter with regard to efficient bacterial cell killing. From their theoretical model, Xue *et al*. suggested that bactericidal efficiency could be enhanced by nanofeatures with larger spacing and/or lower densities. Experimentally, Kelleher *et al.* [25] studied the bactericidal properties of pillar-shaped nanostructures on the wings of 3 different species of cicada. The nanopillars from the 3 samples had varying heights (182-241 nm), pitch (165-251 nm), diameters (156-207 nm), spacings (9-44 nm) and aspect ratios (0.88-1.55), which were tested with a Gram negative bacterium (*P. fluorescens*). They found a correlation which suggested that the greater the number of nanostructures with which the bacterial cells came into contact, the greater the bactericidal activity of the surface. However, the story was complicated by the fact that the

higher death-rate also correlated with the nanopillars having smaller diameters and reduced pitch (*i.e*. they were more densely packed). Dickson *et al.* [26] conducted studies using *E. coli* on nanopatterned PMMA surfaces. They reported that smaller, more closely spaced polymer nanopillars had the best performance. Ivanova *et al.* [27] also recently studied the bactericidal efficacy of bSi against both Gram-positive and Gram-negative bacteria and showed that deformation and cell-wall stress were enhanced with more pronounced, denser nanoprotrusions.

In terms of bacterial cell types, previous work has shown that some nanostructures exhibit a greater bactericidal effect against Gram-negative bacteria than Gram-positive bacteria [28]. It is suggested that this is due to the difference in thickness of the bacterial cell wall. A majority of Gram-positive bacteria have a thicker cell wall with a layer of peptidoglycan that is between 20-80 nm. In contrast, the peptidoglycan layer of most Gram-negative cell walls is much thinner at around 5-10 nm [29]. It is therefore posited that less stress is required to disrupt the cell wall of Gram-negative bacteria, resulting in cell death from purely physical cues [30]. It has also been argued that bacterial motility may play a role in the observed bactericidal effect of a nano-undulating surface, with highly motile bacteria exhibiting a higher death rate on the surface [28]. For these reasons, *E. coli* is often chosen as the model bacterium with which to test bactericidal efficacy. *E. coli* is a motile, rod-shaped Gram-negative bacterium of size ~2 μm by ~0.5 μm, and is a commonly isolated microorganism from nosocomial infections [31]. It is a common coloniser of medical devices such as catheters [32] and is a primary cause of urogenital infections [33]. It has also shown resistance to some antimicrobial therapies [34].

Gram-positive bacteria such as *Staphylococcus aureus* and *Staphylococcus epidermidis* are associated with biomedical-implant-related infections that are difficult to treat and cause fatalities throughout the world [35]. They can colonise surfaces, proliferating and forming dense biofilms. These biofilms are often recalcitrant to antimicrobial therapy, reducing the efficacy of an antibiotic as it cannot penetrate the biofilm to access bacteria located deep within the microcolonies [36]. The Gram-positive bacterium *Streptococcus gordonii* (size ~0.7 μm × 0.5 μm) is a primary coloniser of the human oral cavity and a common constituent of the dental plaque biofilm. As an opportunistic pathogen, *S. gordonii* is also associated with cardiovascular disease infective endocarditis, another condition in which antimicrobial therapy is problematic due to biofilm formation on heart valves [37,38].

In this report, we study bSi and bD surfaces with different needle lengths and packing densities, and investigate their bactericidal effects upon examples of both Gram-negative (*E. coli*) and Gram-positive (*S. gordonii*) bacteria.

3. Experimental

(a) Black silicon fabrication

Three types of bSi substrates were prepared by plasma etching of n-doped single-crystal silicon (100) wafers. The bSi needles were produced in various Oxford Instruments reactive ion etching (RIE) systems fitted with inductively coupled plasma (ICP) sources (see Table 1). Three different ICP etching processes [39] were used, resulting in a bSi wafer of short needles (~0.5 μm in length), a wafer of medium-length needles (~2.5 μm in length), and a wafer of long needles (~20 μm in length), as shown in Figure 1. As well as needle length, the different etching processes produced bSi samples with differing tip diameters and needle densities (see Table 2). For the medium- and long-needle processes, a room temperature process with Cl_2-O_2 was used. For the long-needle process, a cryogenic etch [40,41] using an SF_6-O_2 mixture was used with the wafer electrode cooled to -110°C. Such low temperatures yield very high selectivity of silicon over the micromasking particles, enabling the formation of longer bSi needles. Indeed, the 20-μm needles produced this way are some of the longest bSi features reported to date. All wafers were cleaved into multiple identical square samples ~1 cm^2 in size, suitable for subsequent testing.

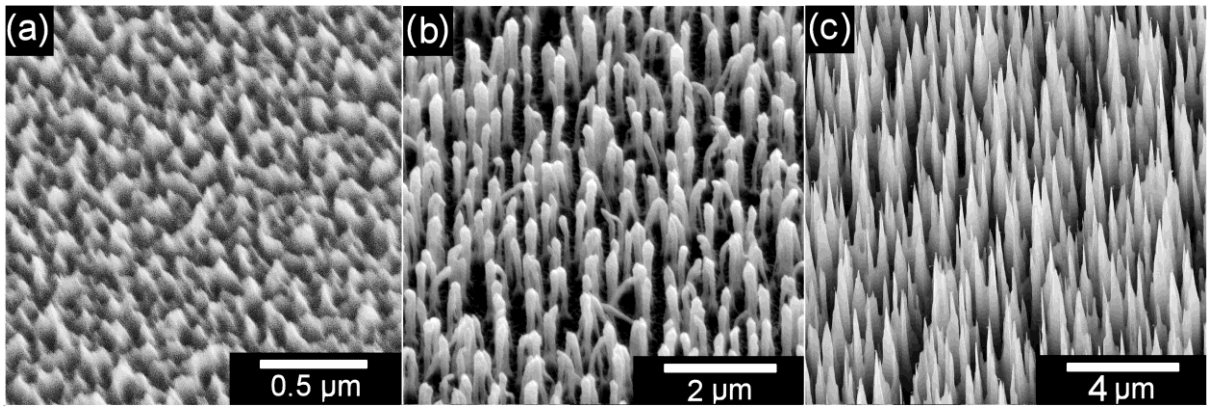

Fig.1. Scanning electron microscope (SEM) images of the bSi needles. (a) Short needles, (b) medium needles, (c) long needles.

Table 1. Fabrication conditions for the bSi needles. The ICP etching reactors were all manufactured and operated by Oxford Instruments Plasma Technology, Ltd [42]. These reactors use inductively coupled radio frequency (RF) power to sustain a plasma, and a second RF power supply capacitively coupled to one electrode (as in a standard RIE system) to induce a DC bias which controls the ion bombardment energy onto the substrate sitting on that electrode. All gases were supplied by B.O.C. and were electronic grade (99.999%).

	Short needles	Medium needles	Long needles
Reactor model, ICP source	System 133, ICP380	System 100, Cobra180	System 100, Cobra300
Etch gases / sccm:			
Cl_2	48	48	0
O_2	15	15	10
SF_6	0	0	60
Pressure / mtorr	15	15	10
ICP power / W	600	600	800
RIE bias power / W	100	50	6
Electrode temp. / °C	20	20	-110
Etching time / min	10	20	30
Backside helium	None	He at 10 torr	He at 10 torr

Table 2. Details of the 3 types of uncoated bSi needles and bD needles, as measured by SEM.

	bSi needles				**bD needles**		
	Short	**Medium**	**Long**		**Short**	**Medium**	**Long**
Needle length / μm	~0.5	~2.5	18-20		~1.0	~3.0	18-20
Tip diameter / nm	< 30	100	< 50		50-100	300-400	300-400
Needle density / μm^{-2}	65	8	1.5		65	8	1.5

(b) Diamond deposition

The bSi samples were seeded using a suspension of ~4-10 nm detonation nanodiamond (DND) in methanol using an electrospray process [43] in which the DND suspension was placed under high potential difference (35 kV) with respect to the grounded sample. Due to electrostatic attraction, the suspension sprayed onto the sample and coated all the surfaces, including the vertical sides of the needles, with a near monolayer of DND seeds. The seeded samples were then placed into a hot filament CVD (HFCVD) reactor and ~0.25 μm of B-doped microcrystalline diamond (MCD) was deposited using standard CVD conditions: 20 Torr pressure, Re filament at 2400 K, substrate temperature ~900°C, 1%CH_4/H_2 +2000 ppm B_2H_6

gas mixture [1,2]. (The films were boron doped to make the diamond layer electrically conducting allowing them to be potentially also used for electrochemical applications, even though such electrochemical applications were not the focus of this project). A growth time of ~60 min allowed a continuous and conformal diamond coating to be deposited without filling in the gaps between the needles. Diamond deposited under these conditions leads to hydrogen termination of the surface, which is hydrophobic and believed to disfavour cell growth, as opposed to oxygen termination which is hydrophilic and enhances cell growth [6].

The resulting bD samples remained deep black due to absorption of visible light, and their microstructure can be seen in Figure 2. Laser Raman analysis of the deposited diamond confirms it is consistent with small-grained CVD diamond (see Supplementary Material). Due to the submicron thickness of the diamond layer, the diamond grain size is small (<100 nm) so the MCD film appears rounded with only small facets visible. The short bSi needles were coated uniformly with diamond to a thickness of ~0.5 μm, leaving a surface which was rounded compared to the uncoated Si needles (Figure 2(a)). The medium and long needles were diamond coated conformally and uniformly all down their length, with complete coverage occurring after 1 h growth (Figure 2(b,c)). After diamond coating, the density of the needles remained unchanged, while the length increased by ~0.5 μm and the tip diameter became significantly less sharp, increasing from 30-100 nm to 300-400 nm. A high-resolution TEM image of the end of one of the needles is shown in figure 2(f). This highlights the core-shell nature of the bD needles with their silicon interior remaining intact and diamond coating with thickness around 150 nm.

As control samples, flat Si substrates were electrospray seeded with DND, and a CVD diamond film deposited onto it under the same conditions as before, except for a time of 8 h. This led to a continuous polycrystalline diamond film ~3 μm thick. Although we shall refer to these samples as ‘flat’ diamond, it should be noted that the surface is faceted from the various randomly oriented diamond crystallites, which gives an overall surface roughness of about 0.2 μm, as seen in Figure 2(e).

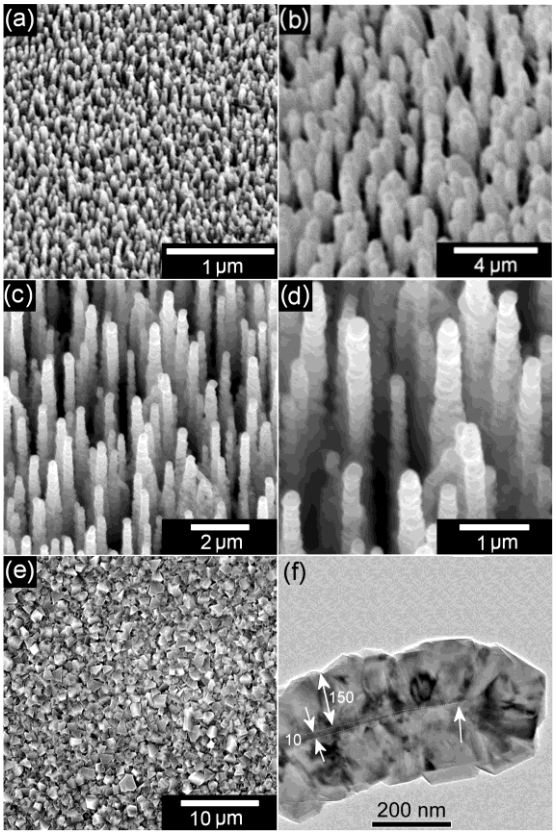

Fig.2. SEM images of the various bD samples (a) short needles, (b) medium needles, (c,d) long needles, (e) the 'flat' diamond control sample and (f) high-resolution TEM image of the end of a bD needle showing core-shell structure. Measurements are in nm. The diamond film thickness is ~150 nm, while the Si needle core is ~10 nm at the left of the picture, tapering to a point at about midway across shown by the right arrow.

(c) Bactericidal surface testing

(i) Bacterial culture preparation

Two bacterial species were used: *E. coli* K12 and *S. gordonii* DL1 (Challis). *E. coli* K12 was grown aerobically for 16 h in 15 ml of Tryptic Soy Broth (TSB, Oxoid) in a 37 °C shaker incubator set at 220 rpm. *S. gordonii* was grown anaerobically for 16 h in Brain Heart Infusion Broth (Lab M) supplemented with 0.5 g L^{-1} yeast extract (BHY) under static conditions in a 37 °C incubator. Bacterial suspensions were then diluted into their respective media to OD_{600} 0.1 and further incubated until mid-exponential phase was reached. Bacterial cells were harvested by centrifugation (7 mins, 5000 *g*), washed twice in 10 mM Tris-HCl buffer, and suspended in Tris-HCl to OD_{600} 0.3 (approximately 10^7 CFU ml^{-1}). Every experiment was

repeated six times, *i.e*. with six identically prepared control, bSi or bD samples, to allow for statistical variability.

(ii) Bacterial adhesion

All test and control surfaces were rinsed with absolute ethanol prior to bacterial adhesion studies. Surfaces were placed into a 12-well microtiter plate and submerged in 2 ml of bacterial suspension. Plates were incubated for 1 h at 37 °C under static conditions. After incubation, surfaces were rinsed to remove non-adherent bacteria by gently holding the surfaces with a pair of tweezers and passing back and forth five times in a uniform manner into a Universal container containing Tris-HCl buffer.

(iii) Live/Dead staining and fluorescence microscopy

After rinsing, 1 ml of Live/Dead® BacLight™ bacterial viability stain was applied to the surfaces according to the manufacturer's instructions. The surfaces were incubated in the dark for 15 mins at room temperature and rinsed in Tris-HCl in the same manner as described above. Bacterial cell viability was then visualized by fluorescence microscopy. *ImageJ* software was used to calculate the number of cells with intact membranes (SYTO 9, stained green) and the number of cells with damaged membranes (propidium iodide, stained red), based on three images per surface performed in triplicate. The average percentage of damaged cells was determined based on three independent studies. A one-way analysis of variance (ANOVA) was performed to compare data sets with *post-hoc* analysis using a two-tailed homoscedastic student's t-test, with $p < 0.05$ considered statistically significant.

(iv) Scanning electron microscopy

To visualise the bacteria by SEM following the 1 h incubation, the bacteria were fixed onto the surface by immersion in 2.5% gluturaldehyde solution (Sigma Aldrich) in 0.1 M potassium phosphate buffer (potassium phosphate monobasic and potassium phosphate dibasic, pH 7.2, Sigma Aldrich) for 2 h at room temperature. The surfaces were then dehydrated by sequential immersion in 20%, 40%, 60%, 80% and 100% ethanol for 10 min each, and finally hexamethyldisilazane for 10 min. The samples were air dried, mounted onto carbon stubs, and sputtered with gold before being viewed by SEM.

4. Results

Representative fluorescence micrographs of *E. coli* after 1 h incubation on various bSi and bD needle samples, plus the flat diamond control sample, are shown in Figure 3. Here, cells with intact membranes are stained green and cells with damaged membranes are stained red.

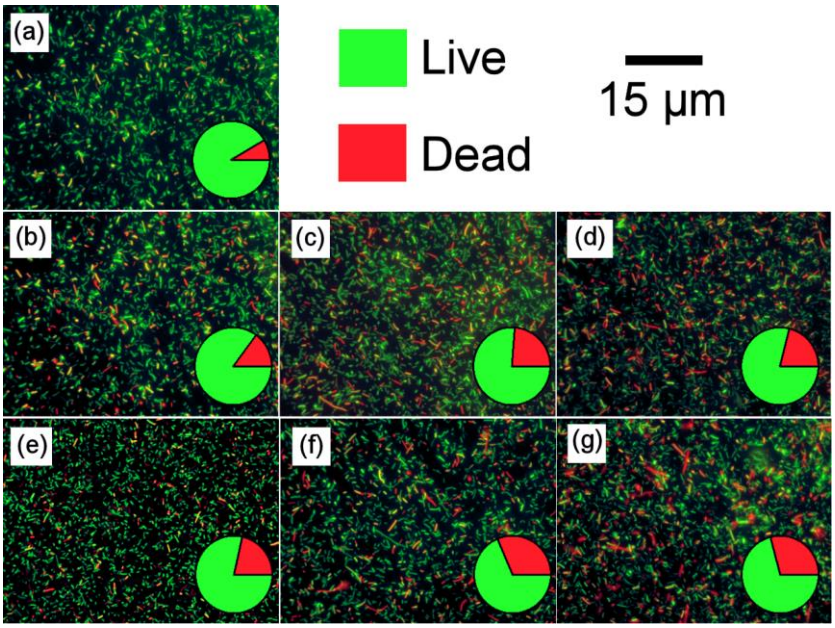

Figure 3. Representative fluorescence micrographs of *E. coli* after 1 h incubation on a) flat diamond control surface, b, c, d) short, medium and long bSi needles respectively and e, f and g) equivalent bD needles. Bacterial cells were stained such that cells with intact membranes (*i.e.* viable cells) fluoresce green and cells with damaged membranes (*i.e.* dead cells) fluoresce red. Pie charts represent the percentages of live and dead cells (green and red, respectively).

From analysis of the fluorescence micrographs in Figure 3 it is clear that attachment of bacteria to the nanostructured bSi and bD surfaces results in significant killing of bacteria when compared to a flat control surface. The percentage of stained dead cells on all surfaces tested in this study is shown in Figure 4.

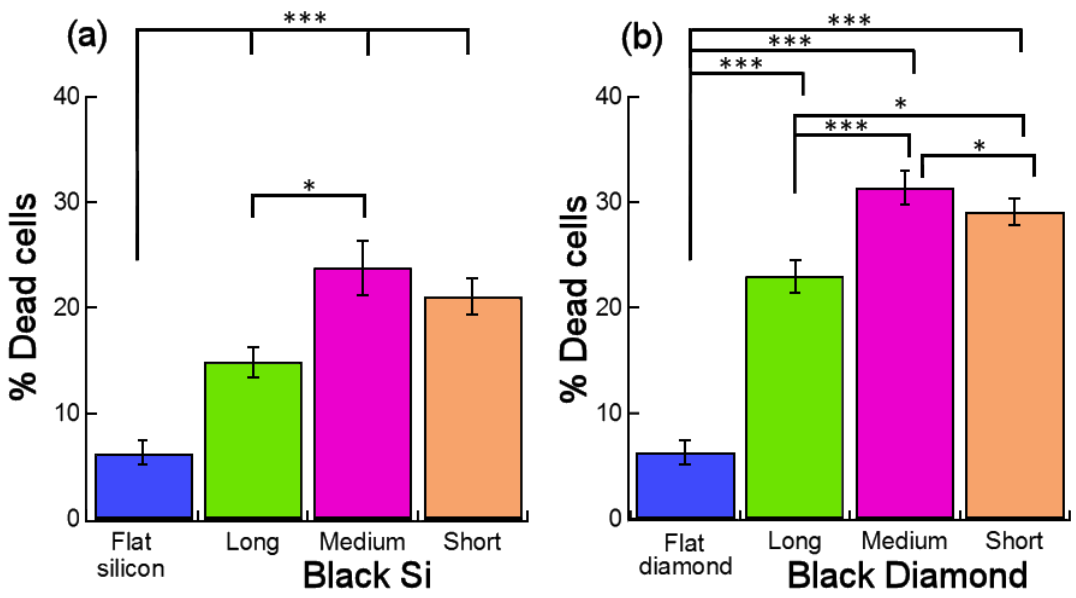

Figure 4. Percentage of dead cells after 1 h incubation of *E. coli* on long, medium and short bSi needles and bD needles along with a flat control. Comparison by ANOVA with a *post-hoc* two-tailed homoscedastic *t*-test to compare individual data sets, with *$p< 0.05$ and ***$p<0.001$.

From analysis of Figure 4, all nanopatterned surfaces result in significant amounts of bacterial killing compared to the flat control surface, which had a percentage of dead cells ~6.3%. Comparing the death rate on bSi and bD needles of the same size, the diamond coating appears to have slightly improved the biocidal activity, although the effect is small given the error bars in the measurements.

For both materials there does not appear to be a linear relationship between needle length and bactericidal efficacy. On both the bSi and bD needle surfaces, the lowest percentage cell death (15-23%) is found on the longest needles (18-20 μm), whilst the highest percentage cell death (24-31%) is found on the medium needles with an average length of 2.5 μm.

However, the same data can be analysed in terms of needle density. Based on the models for cell death outlined in the Introduction, it is expected that the more needles there are in a given area, the greater the opportunity to disrupt the cell membrane and kill bacteria. The long needles (with a density of ~1.5 needles μm^{-2}) kill ~15-23% of the adherent bacteria, whereas the corresponding medium and short needles (with greater densities ~7.8 and 65.2 needles μm^{-2}) kill ~24-31% and 21-24 % of adherent cells, respectively. This can also be interpreted following the rationale of Kelleher *et al*. [25] in terms of the number of needles with which a bacterium interacts. This gives values of ~1-2 interactions for the long needles, ~8 for the

medium needles and ~65 for the short needles. In comparison, Kelleher's group found the highest death rate for ~24 interactions per bacterium, which is generally consistent with our results.

For the Gram-positive bacterium, *S. gordonii*, the bactericidal activity of bSi needle surfaces is distinctly less effective compared to Gram-negative bacterium *E. coli* (Figure 5). This is despite the fact that the number of needle interactions per bacterium is ~23, still close to the optimal values for cell death expected based on the results from *E coli*. On an equivalent surface, the percentage dead cells are 1.5% and 29% for *S. gordonii* and *E. coli*, respectively.

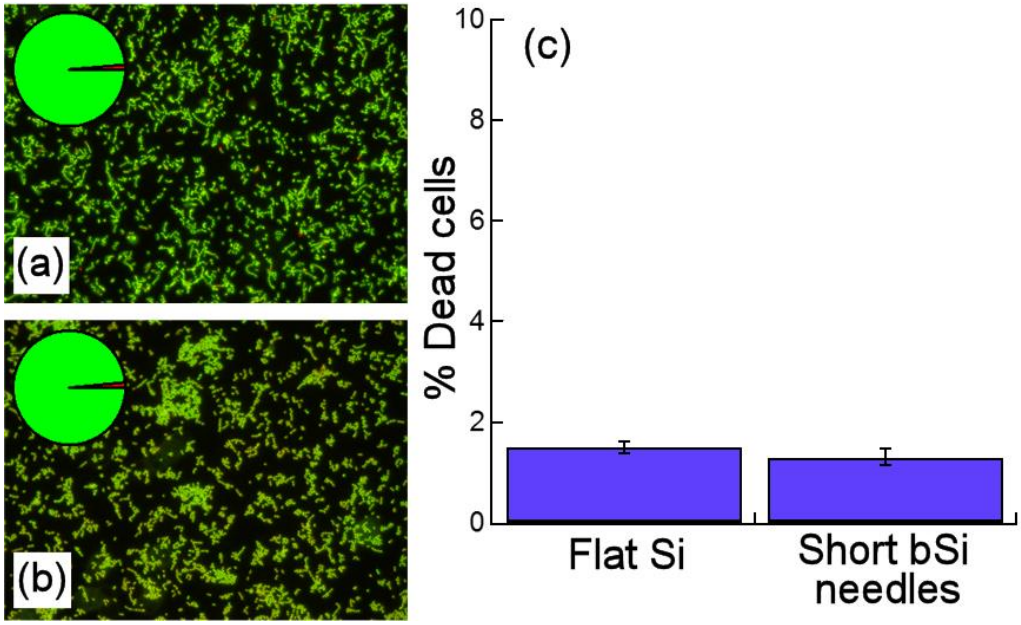

Figure 5. Representative fluorescence micrographs of *S. gordonii* after 1 h incubation on (a) flat Si control surface, (b) short-needle bSi surface. Bacterial cells were stained as before, with green indicating live cells and red indicating dead cells. Pie charts represent the percentages of live and dead cells (green and red, respectively). (c) Percentage cell death for *S. gordonii* on these two surfaces.

In addition to viability staining, equivalent samples were also fixed for visualization by SEM after the 1 h bacterial incubation period, as shown in Figure 6. Many of the cells on the long needles settle in between the gaps of the nanofeatures and appear to display an undamaged morphology (Figure 6a and 6b). However, the sharp tip-width of the bSi long-needle surface appears to directly penetrate the cell causing a loss of turgor pressure, lysis and a flattening of the cell (Figure 6c). Similarly, the shorter needles have a detrimental effect on *E. coli* viability causing the cells to show a damaged morphology (Figure 6e and d). This is in contrast to the

Gram-positive bacteria whereby the cells show a characteristic *cocci* morphology and are beginning to form chain-like structures on the short bSi surfaces.

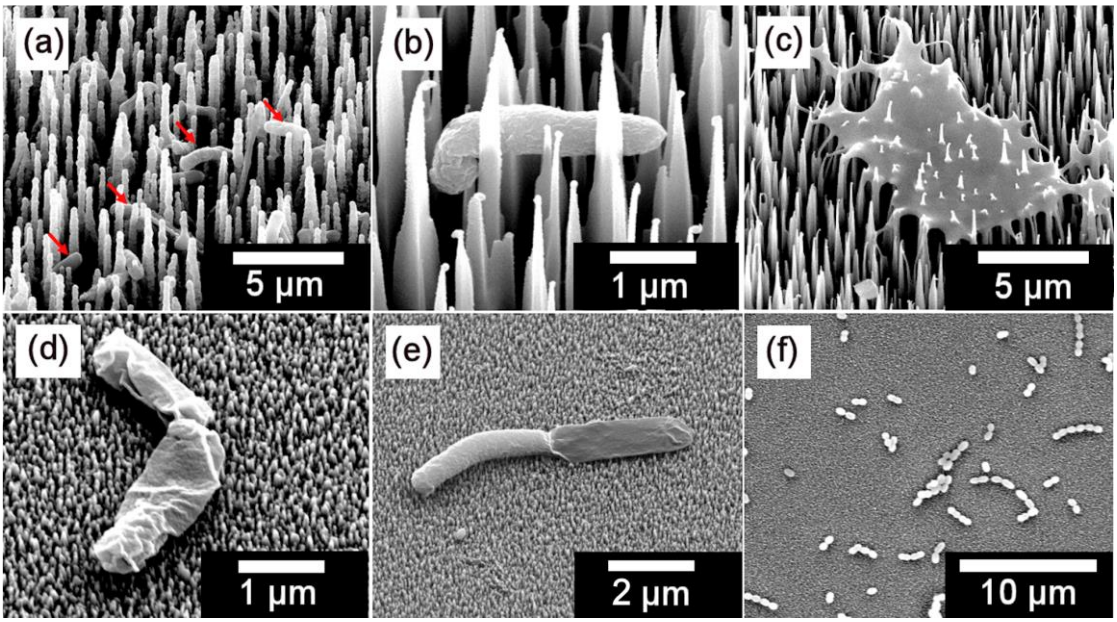

Figure 6. SEM images for *E. coli* after 1 h incubation. (a) bD long needles with bacteria (highlighted by red arrows) lying in the gaps between the sparsely spaced needles. (b) Close-up image of a single bacterium trapped in the gaps between the bSi long needles. (c) bSi long needles with a lysed bacterium impaled by the needles. (d) Short bD needles with unhealthy bacteria. (e) Short bD needles showing one viable and one lysed bacterium. (f) Seemingly viable *S. gordonii* on short-needle bSi surfaces after 1 h incubation.

5. Discussion

The effect of the diamond coating is to round off the ends of the needles, making them less sharp, yet the death rate for the rounded bD needles is arguably slightly higher than that for the sharper bSi needles. This suggests that the mechanism of action causing the cell death may be more complicated than the simple, direct penetration of the cell membrane by the needles.

For the bSi and bD needle surfaces studied here, it is clear that densely packed needles are required to kill higher numbers of bacteria. However, for bD, the surface with the highest density of needles does not kill the highest number of bacteria. The lower death rate on the small bD needle surface (with highest density) relative to the medium needle surface (with

medium density) ($p < 0.05$) may be due to two contributing factors. The first is that the bacterial cell surface interaction is consistent with the mathematical model proposed by Xue *et al* [20]. *E. coli* are ~2 μm in size, for the small needle surfaces which are densely packed this means each cell interacts with ~65 needles. This is insufficient to promote significant stretching of the cell wall and hence produce a lower degree of membrane rupturing. This so-called "bed of nails" effect may provide a more favourable interface due to the highly dense nanostructured surfaces relative to less dense analogues. Secondly, the height of the small needles is the lowest of all surfaces studied here. Smaller height may not allow sufficient stretching/deformation of the cell membrane and a lower percentage death is observed. Together, these two effects may suggest that, despite the higher density for the short needles compared to the medium needles, the kill percentage is slightly lower on the smaller needles. However, data for the analogous bSi surface is not statistically significant and hence the data is still inconclusive. In contrast, at the other end of the length scale, the long, low-density needle surface, with on average only 1 or 2 needle interactions per bacterium, leads to some bacteria lying in the gaps between the needles, rather than being stretched between individual needle tips. This may suggest that there is an optimum density, producing between 1 and 65 interactions per bacterium, with our example in this range being ~8 needles interactions per bacterium, where once reached, the kill rate plateaus or even decreases.

The finding that neither the small bSi nor the bD needles were significantly bactericidal against *S. gordonii* while resulting in significant killing of *E. coli*, despite having a needle interaction value that is nearly optimal at ~23, serves to highlight an important limitation within the field of study. It is generally agreed that the thicker peptidoglycan component of the Gram-positive cell wall inhibits the susceptibility of these bacteria to mechanical rupture by an undulation in nanotopography. The considerably lower kill rate against *S. gordonii* on the small bSi needle surfaces may be due to a combination of the following two factors. First, the thicker cell wall may provide extra rigidity and prevent the bacteria from being pierced and/or stretched. This would lead to the integrity of the cell membrane being maintained, allowing the bacteria to survive on such surfaces. Second, motility has been suggested as a reason for enhanced cell-wall rupture on some nanotextured surfaces [28]. *E. coli* is a motile bacterium meaning that it may attempt to spread itself out on a surface in an attempt to find a more favourable interface. Such motile movement may induce a strain effect across the cell wall, leading to rupture and lysis. By contrast, *S. gordonii* is a non-motile bacterium that grows predominantly in chains. Once attached to a surface, bacterial cells do not significantly move

or spread out, which is likely to place less strain on the cell wall. To confirm these ideas, however, a more detailed study is needed on *S. gordonii*, using different needle lengths and densities optimised for these smaller cells.

6. Conclusions

Black silicon and black diamond needles were fabricated using RIE and CVD techniques. Arrays of nanoneedles were fabricated with differing heights, tip radii and densities. All surfaces generated showed significantly higher levels of bactericidal activity when compared to a flat control surface. A general trend was observed in which surfaces with a higher density of needles killed larger numbers of the Gram-negative bacterium, *E. coli*. However, if the needle density becomes too sparse, the bacteria can settle in the gaps between the needles and are less susceptible to mechanical rupture by interaction with the needles.

The study also served to highlight some of the potential limitations in terms of killing Gram-positive cells. Surfaces with bSi needles were unable to kill large numbers of the Gram-positive bacterium, *S. gordonii*. It is suggested that this is due to the thicker cell wall (peptidoglycan layer) found in Gram-positive cells and a lack of motility. This thicker cell wall is able to withstand higher levels of stress than their Gram-negative counterparts.

In future experiments it may be informative to change the surface chemistry of such interfaces. It is possible to chemically functionalise these bD surfaces with a range of small ions and molecules such as fluorine, hydroxyl, *etc*. This will alter the chemistry, hydrophilicity and energy of the surface, and will serve as an experimental test of some of the mathematical models proposed in the literature in terms of adhesion energy. This is also likely to yield a different response from Gram-positive cells.

However, this study clearly shows that both bSi and bD surfaces can serve to kill adherent Gram-negative bacteria. In real world applications, surfaces that we wish to be bioresistant will probably never be coated with materials as exotic as bSi or bD, but rather be fabricated from more standard materials like titanium or stainless steel. Nevertheless, the principles and information about which types, shapes and densities of surface morphology are optimal for biocidal activity from these studies will be valuable for the generation of new types of antibacterial surfaces made from more practical materials. Because bacteria come in many different sizes, practical biocidal surfaces may need to have a range of nanofeatures with different sizes and densities to affect simultaneously a broad spectrum of bacteria.

7. Acknowledgements.

The authors thank the Electron Microscope Unit at the University of Bristol, School of Chemistry, for use of their facilities, and to Ed Smith and Jean-Charles Eloi for taking the TEM image. The authors also thank the EPSRC BristolBridge award: Bridging the Gaps between the Engineering and Physical Sciences and Antimicrobial Resistance (grant EP/M027546/1) and the MRC (Innovation Grant (MR/N010345/1)) for funding these trials of antimicrobial surfaces. Supplementary material and raw data for this report can be found in the University of Bristol data repository: DOI: {add this at proofs stage}

8. Declarations

Declarations of interest: none. All authors have approved the final article. The bSi fabrication was done by CCW, the CVD diamond deposition and characterisation was done by PT supervised by PWM. Bactericidal experiments were performed by PT, GH and AHN, with BS as supervisor. The manuscript was written by GH and PWM.

References

1. May, P. W., Diamond thin films: A 21st century material. *Philosophical transactions of the Royal Society London A* **2000**, *358*, 473.
2. May, P. W.; Ludlow, W. J.; Hannaway, M.; Heard, P. J.; Smith, J. A.; Rosser, K. N., Raman and conductivity studies of boron doped microcrystalline diamond, facetted nanocrystalline diamond and cauliflower diamond films. *Diamond Related Materials* **2008**, *17*, 105.
3. Yang, N.; Foord, J.; Jiang, X., Diamond electrochemistry at the nanoscale: A review. *Carbon* **2016**, *99*, 90-110.
4. Macpherson, J. V., A practical guide to using boron doped diamond in electrochemical research. *Physical Chemistry Chemical Physics* **2015**, *17*, 2935.
5. Utrilla, M.; Polo, M.; Garcia, M.; Joya, G.; Perez, R., Pharmaceuticals as emerging contaminants and their removal from water. A review. *Chemosphere* **2013**, *93*, 1268.
6. Nistor, P. A.; May, P. W.; Tamagnini, F.; Randall, A. D.; Caldwell, M. A., Long-term culture of pluripotent stem cell derived human neurons on diamond- a substrate for neurodegeneration research and therapy. *Biomaterials* **2015**, *61*, 139-149.
7. Nistor, P. A.; May, P. W., Diamond thin films: giving biomedical applications a new shine. *Journal of the royal society interface* **2017**, *14*, 20170382.
8. Moreira, J. V. S.; May, P. W.; Corat, E. J.; Peterlevitz, A. C.; Pinheiro, R. A.; Zanin, H., Diamond and nanocarbon composites for supercapacitor devices. *Journal of Electronic Materials* **2016**, 1-7.
9. Zanin, H.; May, P. W.; Fermin, D. J.; Plana, D.; Vieira, S. M. C.; Milne, W. I.; Corat, E. J., Porous boron-doped diamond/carbon nanotube electrodes. *ACS Applied materials and interfaces* **2013**, *6* (990).
10. Yang, N.; Uetsuka, H.; Williams, O. A.; Osawa, E.; Tokuda, N.; Nebel, C. E., Vertically aligned diamond nanowiresxx: Fabrication, characterisation and application for DNA sensing. *Physica Status Solidi A* **2009**, *206*, 2048-2056.
11. May, P. W.; Clegg, M.; Silva, T. A.; Zanin, H.; Fatibello-Filho, O.; Celorrio, V.; Fermin, D. J.; Welch, C. C.; Hazell, G.; Fisher, L. E.; Nobbs, A. H.; Su, B., Diamond coated 'black-silicon' as a promising material for high surface-area electrochemical electrodes and antibacterial surfaces. *Journal of materials Chemistry B* **2016**, *4*, 5737-5746.

12. Oh, J.; Yuan, C.; Branz, H. M., An 18.2%-efficient black-silicon solar cell acheived through control of carrier recombination in nanostructures. *Nature Nanotechnology* **2012**, *7*, 743-748.
13. Roy, A. B.; Dhar, A.; Choudhuri, M.; Das, S.; Hossain, S. M.; Kundu, A., Black silicon solar cell: analysis optimization and evolution towards a thinner and flexible future. *Nanotechnology* **2016**, *27*, 305302.
14. Kim, W.; Ng, J. K.; Kunitake, M. E.; Conklin, B. R.; Yang, J., Interfacing silicon nanowires with mammalian cells. *Journal of the American Chemical Society* **2007**, *129*, 7228-7229.
15. Shalek, A. K.; Robinson, J. T.; Karp, E. S.; Lee, J. S.; Ahn, D. R.; Yoon, M. H.; Sutton, A.; Jorgolli, M.; Gertner, R. S.; Gujral, T. S.; MacBeath, G.; Yang, E. G.; Park, H., Vertical silicon nanowires as a universal platform for delivering biomolecules into living cells. *Proceedings of the National Academy of Sciences* **2010**, *107*, 1870-1875.
16. Ivanova, E. P.; Hasan, J.; Webb, H. K.; Gervinskas, G.; Juodkazis, S.; Truong, V. K.; Wu, A. H. F.; Lamb, R. N.; Baulin, V. A.; Watson, G., S; Watson, A. J.; Mainwaring, D. E.; Crawford, R. J., Bactericidal activity of black silicon. *Nature Communications* **2013**, *4*, 2838.
17. Al-Jumaili, A.; Alancherry, S.; Bazaka, K.; Jacob, M. V., Review on the antimicrobial properties of carbon nanostructures. *Materials* **2017**, *10*, 1065-
18. Ivanova, E. P.; Hasan, J.; Webb, H. K.; Truong, V. K.; Watson, G. S.; Watson, J. A.; Baulin, V. A.; Pogodin, S.; Wang, J. Y.; Tonbin, M. J.; Lobbe, C.; Crawford, R. J., Natural bactericidal surfaces: Mechanical rupture of *pseudomonas aeruginosa* cells by cicada wings. *Small* **2012**, *8*, 2489-2494.
19. Pogodin, S.; Hasan, J.; Baulin, V. A.; Webb, H. K.; Truong, V. K.; Phong Nguyen, T. H.; Boshovikj, V.; Fluke, C. J.; Watson, G., S; Watson, A. J.; Crawford, R. J.; Ivanova, E. P., Biophysical model of bacterial cell interactions with nanopatterned cicada wing surfaces. *Biophysical Journal* **2013**, *104*, 835-840.
20. Xue, F.; Liu, J.; Guo, L.; Zhang, L.; Li, Q., Theoretical study on the bactericidal nature of nanopatterned surfaces. *Journal of Theoretical Biology* **2015**, *385*, 1-7.
21. Li, X., Bactericidal mechanism of nanopatterned surfaces. *Physical Chemistry Chemical Physics* **2016**, *18*, 1311-1316.
22. Nowlin, K.; Boseman, A.; Covell; Abeles, F.; LaJeunesse, O., Adhesion dependent rupturing of saccharomyces cerevisiae on biological nanostructured surfaces. *Journal of the Royal Society Interface* **2015**, *12*, 20140999.

23. Bandara, C. D.; Singh, S.; Afara, I. O.; Wolff, A.; Tesfamichael, T.; Ostrikov, K.; Oloyede, A., Bactericidal effects of natural nanotopography of dragonfly wing on Escherichia coli. *ACS Applied Materials and Interfaces* **2017**, *9*, 6746-6760.
24. Wu, S.; Zuber, F.; Brugger, J.; Maniura-Weber, K.; Ren, Q., Antibacterial Au nanostructured surfaces. *Nanoscale* **2016**, *8*, 2620.
25. Kelleher, S. M.; Habimana, O.; Lawler, J.; O'Reilly, B. O.; Daniels, S.; Casey, E.; Cowley, A., Cicada wing surface topography: An investigation into the bactericidal properties of nanostructural features. *ACS Applied Materials and Interfaces* **2015,** *8*, 14966-14974.
26. Dickson, M. N.; Liang, E. I.; Rodriguez, L. A.; Vollereaux, N.; Yee, A. F., Nanopatterned polymer surfaces with bactericidal properties. *Biointerphases* **2015**, *10*, 0210101-0210108.
27. Linklater, D. P.; Nguyen, H. K. D.; Bhadra, C. M.; Juodkazis, S.; Ivanova, E. P., Influence of nanoscale topology on bactericidal efficiency of black silicon surfaces. *Nanotechnology* **2017**, *28*, 245301.
28. Diu, T.; Faruqui, N.; Sjostrom, T.; Lamarre, B.; Jenkinson, H. F.; Su, B.; Ryadnov, M. G., Cicada-inspired cell-instructive nanopatterned arrays. *Scientific Reports* **2014**, *4* (7122), 1-7.
29. Brown, L.; Wolf, J. M.; Prados-Rosales, R.; Casadevall, A., Through the wall: extracellular vesicles in Gram positive bacteria, mycobacteria and fungi. *Nature Reviews Microbiology* **2015**, *13*, 620-630.
30. Fisher, L. E.; Yang, Y.; Yuen, M.; Zhang, W.; Nobbs, A. H.; Su, B., Bactericidal activity of biomimetic diamond nanocone surfaces. *Biointerphases* **2016**, *11*, 0110141-0110146.
31. Bereket, W.; Hemalatha, K.; Getenet, B.; Wondwossen, T.; Solomon, A.; Zeynudin, A.; Kannan, S., Update on bacterial nosocomial infections. *European Review for Medical and Pharmacological Sciences* **2012**, *16*, 1039-1044.
32. Costerton, J. W.; Stewart, P. S.; Greenberg, E. P., Bacterial biofilms: a common cause of persistent infections. *Science* **1999**, *284*, 1318-1322.
33. Beloin, C.; Roux, A.; Ghigo, J. M., Escherichia coli biofilms. *Current Topics in Microbiology and Immunology* **2008**, *322*, 249-289.
34. Karlowsky, J. A.; Kelly, L. J.; Thornsberry, C.; Jones, M. E.; Sahm, D. F., Trends in antimicrobial resistance among urinary tract infection isolates of Escherichia coli from female outpatients in the United States. *Antimicrobial Agents and Chemotherapy* **2002**, *46*, 2540-2545.

35. Arciola, C. R.; Campoccia, D.; Speziale, P.; Montanaro, L.; Costerton, J. W., Biofilm formation in Staphylococcus implant infections. A review of molecular mechanisms and implications for biofilm-resistant materials. *Biomaterials* **2012**, *33*, 5967-5982.
36. Huang, C. T.; Yu, F. P.; McFeters, G. A.; Stewart, P. S.; Huang, C.; Yu, F. P., Non-uniform spatial patterns of respiratory activity within biofilms during disinfection. *Applied Environmental Microbiology* **1995**, *61*, 2252-2256.
37. Nobbs, A. H.; Lamont, R. J.; Jenkinson, H. F., Streptococcus adherence and colonization. *Microbiology and Molecular Biology Reviews* **2009**, *73*, 407-450.
38. Keane, C.; Petersen, H. J.; Tilley, D.; Haworth, J.; Cox, D.; Jenkinson, H. F.; Kerrigan, S. W., Multiple sites on streptococcus gordonii surface protein PadA bind to platelet GPIIbIIIa. *Thrombosis and Haemostasis* **2013**, *110*, 1278-1287.
39. Donnelly, V. M.; Kornblit, A., Plasma etching: Yesterday, today and tomorrow. *Journal of Vacuum Science and Technology A* **2013**, *31*, 050825.
40. Welch, C. C.; Goodyear, A. L.; Wahlbrink, T.; Lemme, M. C.; Mollenhauer, T., Silicon etch process options for micro- and nanotechnology using inductively coupled plasmas. *Microelectronics Engineering* **2006**, *83*, 1170-1173.
41. Henry, M. D.; Welch, C. C.; Scherer, A., Techniques of cryogenic reactive ion etching in silicon for fabrication sensors. *Journal of Vacuum Science and Technology A* **2009**, *27*, 1211-1216.
42. Oxford Instruments Plasma Technology, Ltd website. https://www.oxford-instruments.com/businesses/nanotechnology/plasma-technology
43. Fox, O. L. J.; Holloway, J. O. P.; Fuge, G. M.; May, P. W.; Ashfold, M. N. R., Electrospray deposition of diamond nanoparticle nucleation layers for subsequent CVD diamond growth. *Materials Research Society Symposium Proceedings* **2010,** *1203*, J17.